AMERICAN SOCIETY FOR MICROBIOLOGY | Journal of Virology®

STRUCTURE AND ASSEMBLY

Clustered Lysine Residues of the Canine Distemper Virus Matrix Protein Regulate Membrane Association and Budding Activity

Nicole P. Kadzioch,[a,b,c] Matthieu Gast,[a,b,c] Francesco Origgi,[d] Philippe Plattet[a,b]

[a]Division of Experimental Clinical Research, DCR-VPH, Vetsuisse Faculty, University of Bern, Bern, Switzerland
[b]Division of Neurological Sciences, DCR-VPH, Vetsuisse Faculty, University of Bern, Bern, Switzerland
[c]Graduate School for Cellular and Biomedical Sciences, University of Bern, Bern, Switzerland
[d]Centre for Fish and Wildlife Health (FIWI), Department of Infectious Diseases and Pathobiology, Vetsuisse Faculty, University of Bern, Bern, Switzerland

ABSTRACT The canine distemper virus (CDV) matrix (M) protein is multifunctional; it orchestrates viral assembly and budding, drives the formation of virus-like particles (VLPs), regulates viral RNA synthesis, and may support additional functions. CDV M may assemble into dimers, where each protomer is constituted by N-terminal and C-terminal domains (NTD and CTD, respectively). Here, to investigate whether electrostatic interactions between CDV M and the plasma membrane (PM) may contribute to budding activity, selected surface-exposed positively charged lysine residues, which are located within a large basic patch of CTD, were replaced by amino acids with selected properties. We found that some M mutants harboring amino acids with neutral and positive charge (methionine and arginine, respectively) maintained full functionality, including proper interaction and localization with the PM as well as intact VLP and progeny virus production as demonstrated by employing a cell exit-complementation system. Conversely, while the overall structural integrity remained mostly unaltered, most of the nonconservative M variants (carrying a glutamic acid; negatively charged) exhibited a cytosolic phenotype secondary to the lack of interaction with the PM. Consequently, such M variants were entirely defective in VLP production and viral particle formation. Furthermore, the proteasome inhibitor bortezomib significantly reduced wild-type M-mediated VLP production. Nevertheless, in the absence of the compound, all engineered M lysine variants exhibited unaffected ubiquitination profiles, consistent with other residues likely involved in this functionally essential posttranslational modification. Altogether, our data identified multiple surface-exposed lysine residues located within a basic patch of CDV M-CTD, critically contributing to PM association and ensuing membrane budding activity.

IMPORTANCE Although vaccines against some morbilliviruses exist, infections still occur, which can result in dramatic brain disease or fatal outcome. Postexposure prophylaxis with antivirals would support global vaccination campaigns. Unfortunately, there is no efficient antiviral drug currently approved. The matrix (M) protein of morbilliviruses coordinates viral assembly and egress through interaction with multiple cellular and viral components. However, molecular mechanisms supporting these functions remain poorly understood, which preclude the rationale design of inhibitors. Here, to investigate potential interactions between canine distemper virus (CDV) M and the plasma membrane (PM), we combined structure-guided mutagenesis of selected surface-exposed lysine residues with biochemical, cellular, and virological assays. We identified several lysines clustering in a basic patch microdomain of the CDV M C-terminal domain, which contributed to PM association and budding activity. Our findings provide novel mechanistic information of how morbilliviruses

Citation Kadzioch NP, Gast M, Origgi F, Plattet P. 2021. Clustered lysine residues of the canine distemper virus matrix protein regulate membrane association and budding activity. J Virol 95:e01269-20. https://doi.org/10.1128/JVI.01269-20.

Editor Rebecca Ellis Dutch, University of Kentucky College of Medicine

Address correspondence to Philippe Plattet, philippe.plattet@vetsuisse.unibe.ch.

Received 23 June 2020
Accepted 3 October 2020
Accepted manuscript posted online 7 October 2020
Published 9 December 2020

assemble and egress from infected cells, thereby delivering bases for future antiviral drug development.

KEYWORDS *Morbillivirus* cell exit, matrix protein, lysine residues, cell periphery accumulation, membrane association, VLP production

Measles virus (MeV) and canine distemper virus (CDV), two members of the genus *Morbillivirus* within the family *Paramyxoviridae*, are associated with severe impacts on human and animal populations, respectively (1, 2). Both of these infectious agents are enveloped, nonsegmented, single-stranded, and negative-sense RNA viruses. Their genome encodes for six structural (nucleocapsid [N], phosphoprotein [P], matrix [M], fusion [F], attachment [H], and polymerase [L]) proteins as well as two nonstructural accessory elements, the V and C proteins. Multiple units of N protein encapsidate the viral RNA genome, which in turn forms a helical structure enabling the RNA-dependent RNA polymerase (vRdRp; composed of L+P) to dock on. This large complex, also termed the ribonucleoprotein (RNP), represents the minimal infectious unit (3). The viral envelope H glycoprotein binds to a specific host cell receptor, which initiates the cell entry process by activating the interacting fusion glycoprotein. Upon activation, the F protein dramatically refolds and merges the viral envelope with the host cell plasma membrane (PM), thereby generating a fusion pore allowing for the injection of the RNP into the host cell cytoplasm (4–14). The signaling lymphocyte activation molecule (SLAM or CD150) on immune cells and nectin-4 on epithelial cells act as specific MeV and CDV receptors, respectively (15–24). C and V are involved in RNA synthesis as well as in counteracting the antiviral immune cell response. Morbilliviruses replicate in the cytoplasm and exit the cell by employing a budding process proposed to occur at the host cell plasma membrane, a molecular mechanism where the matrix (M) protein plays a pivotal role (3).

The M protein is a major structural protein interacting with the viral envelope. It not only orchestrates viral assembly and budding but also regulates viral RNA synthesis. Moreover, expression of M protein alone in the cell can lead to the formation of virus-like particles (VLPs) either in the presence or absence of other viral components (3, 25–32). Supporting an important role of the M protein in viral assembly, so-called "matrix-less" recombinant MeVs were severely impaired in viral particle formation. Furthermore, such engineered recombinant viruses exhibited enhanced cell-cell fusion, implying a potential role of M in fusion regulation (33). Importantly, M proteins of some related paramyxoviruses and pneumoviruses (e.g., respiratory syncytial virus [RSV], Newcastle disease virus [NDV], Nipah virus [NiV], Hendra virus [HeV], Sendai virus [SeV], or Mumps virus [MuV]) were also documented to traffic through the nucleus. This specific transport mechanism relied on a bipartite nuclear localization signal (NLS) as well as a leucine-rich nuclear export signal (NES). Additionally, ubiquitination of a lysine residue within the NLS, presumptively modified in the nucleus, is assumed to play a key role in viral particle formation (34–41). Intriguingly, such transient nuclear trafficking could not be illustrated in case of morbilliviruses M proteins (42).

To recruit viral factors and initiate assembly at the PM, it is assumed that the M protein interacts with the cytoplasmic tails of H and F glycoproteins as well as with the C-terminal end of N proteins (RNP complex). In addition, interaction of M with the actin cytoskeleton occurs in many viral infections (33, 43–53). For instance, electron microscopy (EM) studies revealed the association of MeV M and actin filaments during budding, where they facilitate the intracellular transport of M-RNP complexes (54). Moreover, downregulation of MeV and CDV budding in the presence of actin polymerization inhibitors was reported, further underlining the critical role of actin filaments during viral assembly (47–49).

Currently, no high-resolution structural data are available for any of the morbillivirus M proteins. However, crystallographic studies of the related NDV, RSV, HeV, and human metapneumovirus (hMPV) M proteins illustrated high structural conservation (27, 55–58). The architecture comprises two similarly folded β-sandwich domains, connected by

an unstructured linker. Two protomers, each composed of amino- and carboxy-terminal domains (NTD and CTD, respectively), assemble in a "head-to-tail" fashion through a large dimeric binding interface (27, 56–59). Multimerization of stable M dimers into a grid-like array at the inner surface of the PM is proposed to drive membrane curvature and formation of viral budding platforms. Both NTD and CTD were proposed to contribute to the formation of high-order oligomers putatively through two surface-exposed α-helices (namely, α2 in NTD and α9 in CTD) located at opposite sides of the dimeric binding interface (27, 56, 57, 59, 60). Interestingly, cryo-electron tomography (cryo-ET) studies revealed an organization of MeV M as a potentially two-dimensional (2D) paracrystalline array. This array was suggested to coordinate contacts between the surface F and H glycoproteins as well as with RNP complexes, thereby contributing in shaping the overall particle architecture (61). However, although this study revealed important structural data, the limited resolution precluded precise mapping of protein-protein interactions and awaits next-generation technologies for validation. Furthermore, another recent structural study revealed that MeV particles may assume an alternative organization, where M proteins form helices coating the RNP complex rather than interacting with the inner leaflet of the viral envelope (54).

The inner leaflet of the PM is enriched in anionic phospholipids, which provide platforms for proteins to mediate membrane association by using surface-exposed positively charged residues. A number of related virus M proteins (e.g., RSV, NDV, and hMPV) are known to bind membranes or lipid vesicles, most likely through a combination of hydrophobic and electrostatic interactions (26, 27, 56, 62–64). Additionally, some matrix proteins of filoviruses, including Ebola virus (EBOV) and Marburg virus, which belong to the same order as paramyxoviruses (i.e., *Mononegavirales*), interact with the inner leaflet of the PM via electrostatic interactions (65–71). Coarse-grained molecular dynamics simulation revealed that cationic patch residues, especially lysine residues, mediate the interaction between EBOV-VP40 and the PM (72).

In the present study, we aimed to gain functional insights into the inherent functions of CDV M that are necessary for cell exit. Based on a previously generated homology three-dimensional (3D) model, we performed a structure-guided mutagenesis approach, which targeted surface-exposed positively charged lysine residues located within M-CTD. The derivative mutants underwent biochemical, cellular, and virological analyses. Altogether, our data identified multiple lysine residues of CDV M-CTD as key regulators of the cornerstone processes of the viral cycle, including cellular localization, membrane association, budding activity, and infectious particle production, while not directly contributing to self-assembly and ubiquitination processes.

RESULTS

Nonconservative M-CTD lysine mutants failed to accumulate at the cell periphery. Recent structural studies highlighted a network-like assembly of the measles matrix protein beneath the PM and the viral envelope (61). Although important insights were provided, the resolution achieved by the technology available could not determine microdomains contributing to M dimer-dimer contacts or even how M dimers spatially organize with regard to the PM. Here, to gain further knowledge on diverse M functions and spatial positioning, we aimed at determining domains of CDV M that may interact with the inner leaflet of the PM. By employing a previously determined homology 3D structural model of the M dimer (27, 59), a large and uniform surface-exposed basic patch, located within the CTD of each M promoter, was unambiguously highlighted (Fig. 1A and B).

Consistently with the proposed electrostatic membrane, interactions for other envelope virus matrix-like proteins (i.e., paramyxoviruses, pneumoviruses, filoviruses), all positively charged lysine residues (K) residing within the basic patch of the CDV M-CTD, were subjected to site-directed mutagenesis (Fig. 1C and D). The targeted lysine residues were replaced by (i) arginine (R; positive charge, conservative mutation), (ii) glutamic acid (E; negative charge, nonconservative mutation), and (iii) methionine (M;

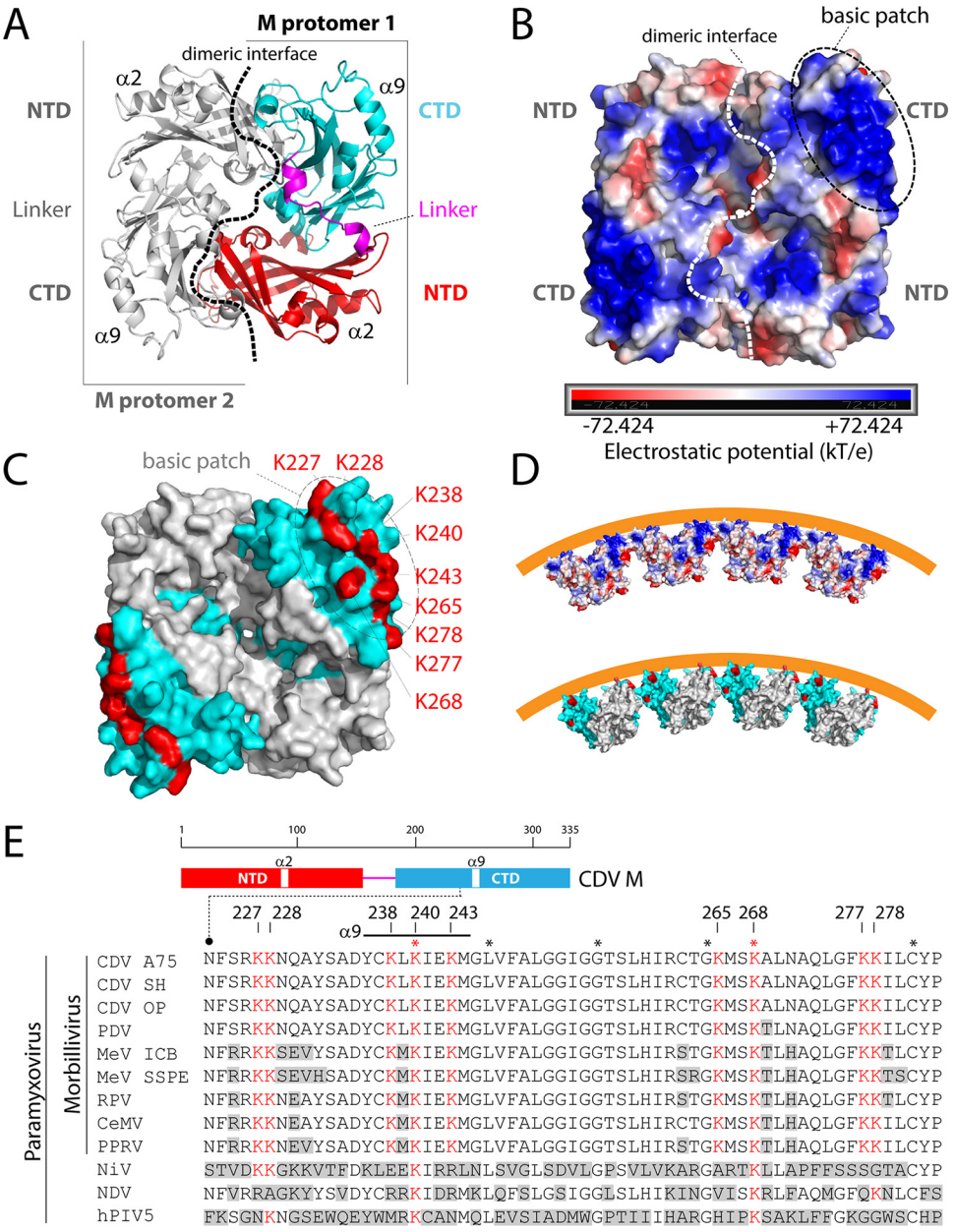

FIG 1 Structural model of CDV M and putative electrostatic interaction via surface-exposed, positively charged, lysine residues. (A) NDV-based (PDB code 4G1G) structural homology model of a CDV M dimer. The three major domains of a protomer are colored in red (NTD), pink (linker), and blue (CTD). Surface-exposed helices, proposed to be involved in dimer-dimer interactions, are labeled as α2 and α9. The promoter-promoter binding interface is highlighted with a dashed black line (59). (B) Electrostatic potential at the molecular surface of CDV M, ranging from blue (+72.424kT/e) to red (−72.424kT/e). The basic patch is indicated. (C) Surface-exposed positively charged lysine residues within the basic patch of the CTD (blue) are highlighted in red. (D) One-directional representation of plasma membrane association via electrostatic interaction (26, 27, 72). (E) Sequence alignment of M proteins of representative paramyxoviruses. At the top is a schematic representation of the M protein's main domains and highlighted lysine residues targeted for mutagenesis. Accession numbers (GenBank or NCBI) for the virus sequences are as follows: CDV A75/17 (CDV A75), AAD49701; CDV Snyder Hill (CDV SH), AFC40215; CDV Onderstepoort (CDV OP), NP_047204; phocine distemper virus (PDV), AGL33552; MeV IC-B (MeV ICB), BAM36454; MeV genotype B3, an SSPE strain (MeV SSPE), ALL29057; rinderpest virus (RPV), CAA53779; cetacean morbillivirus (CeMV), AEO51054; peste-des-petits-ruminants virus (PPRV), ACQ44669; Nipah virus (NiV), NP_112025; Newcastle disease virus (NDV), AEZ36128; and human parainfluenza virus 5 (hPIV5), ABC75775. The stars represent amino acids conserved throughout members of the subfamily. Amino acids differing from the reference CDV M sequence (strain A75/17) are shown in gray boxes.

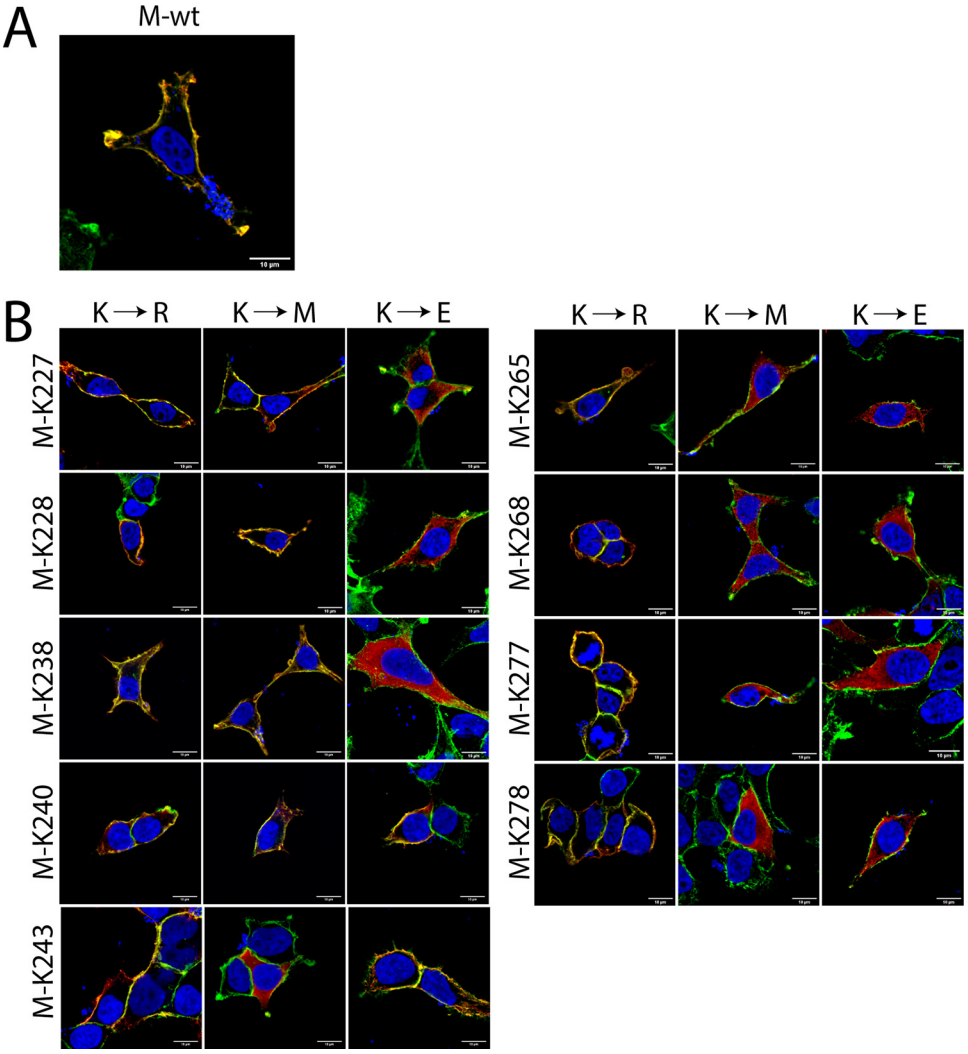

FIG 2 Cellular localization of CDV M mutants. FLAG-tagged M wt (A) and M mutant proteins (B) were expressed in HEK-293T cells, and cellular localization was investigated by immunofluorescence analysis after 24 h. FLAG-tagged M proteins were stained in red, and the PM and nuclei were counterstained in green and blue, respectively.

neutral charge, similar in structure to lysine). Of note, the selected lysine residues are well conserved among all members of the *Morbillivirus* genus, with some even broadly in paramyxoviruses (Fig. 1E).

To investigate the impact of the rationally designed M mutants on intracellular localization, immunofluorescence analyses were performed. To highlight the cell periphery, plasma membranes were counterstained with an antibody targeting the PM-residing alpha 1 subunit of the sodium-potassium pump. In accordance with our previous study (59), wild-type (wt) M proteins were efficiently transported to the cell periphery (Fig. 2A). Likewise, the conservative M mutants exhibited similar phenotypes (Fig. 2B, left panels). In contrast, the nonconservative M variants exhibited a clear cytosolic phenotype, except for M-K240E and M-K243E, which preserved cell periphery localization (Fig. 2B, right panels). The methionine mutants, M-K227M, -K228M, -K238M, and -K240M were efficiently transported to the cell periphery, whereas the others (M-K243M, -K265M, -K268M, -K277M, and -K278M) showed a location consistent with a cytosolic phenotype (Fig. 2B, panel 2). Taken together, immunofluorescence analyses revealed that most of the nonconservative M variants exhibited a cytosolic phenotype presumably secondary to the lack of interaction with the PM. Conversely, conservative M mutants revealed proper localization with PM indirectly supporting the critical role of positively charged residues.

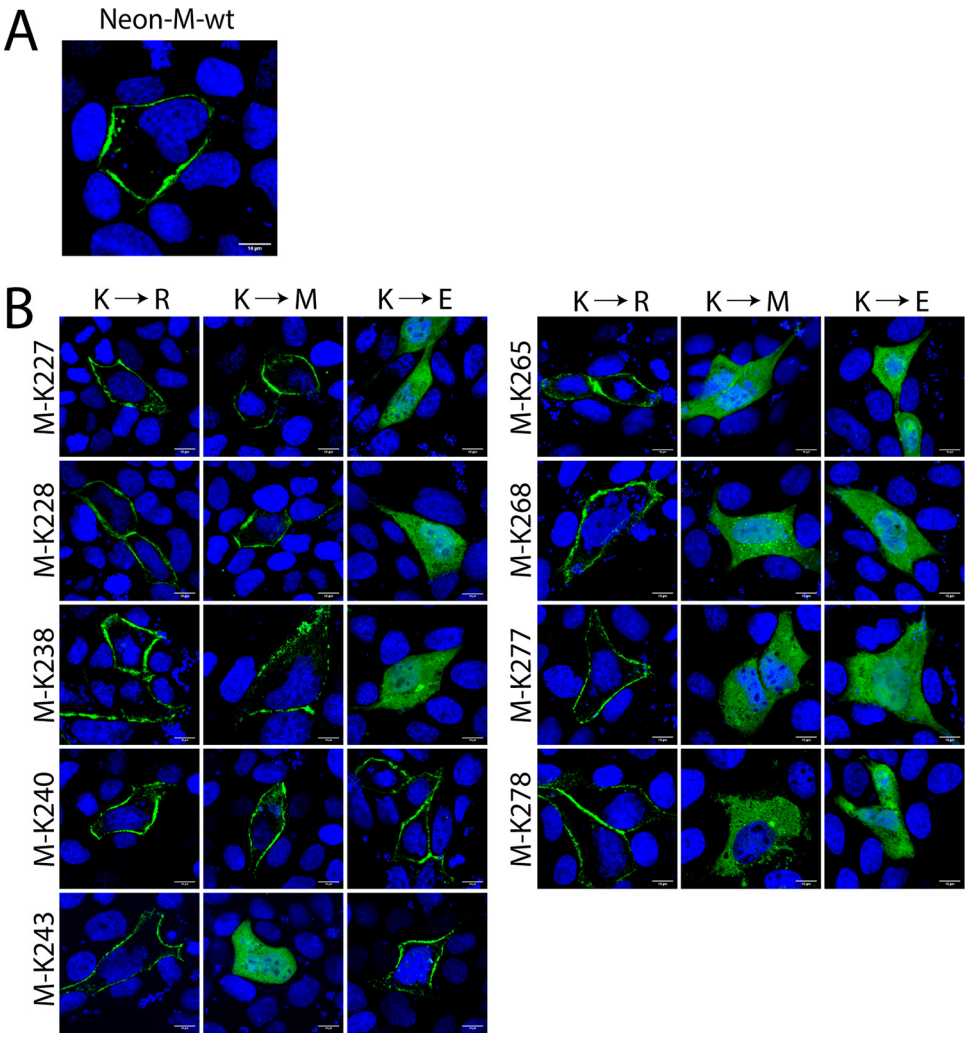

FIG 3 Cellular localization of CDV mNeonGreen-M mutants. mNeonGreen-tagged M-wt (A) and M-mutant (B) proteins were expressed 24 h in MDCK cells, and cellular localization was investigated by fluorescence analysis. Nuclei were counterstained with DAPI.

Interestingly, M-K240E and M-K243E preserved cell periphery localization despite harboring nonconservative amino acid changes (Fig. 2B). However, both residues are potentially located within the M-CTD α9-helix, a microdomain proposed to rather contribute in self-assembly (27, 59). Accordingly, those two mutants were excluded from this study, and the next biochemical and functional analyses were then focused on M lysine mutants, which unequivocally exhibited a lack of cell periphery accumulation when carrying nonconservative substitutions. Specifically, for M-K238E (which also featured cytosolic accumulation), our 3D model suggested that residue at position 238 of CDV M might be buried deeper inside the protein, thereby putatively affecting protein folding and, eventually, cellular localization. This potential difference warranted a separate analysis of M-K238E.

In addition, to investigate the impact of CDV M mutants on intracellular localization in a canine cell line, fluorescence analyses with mNeonGreen-tagged M mutants were performed in MDCK (Madin-Darby canine kidney) cells (Fig. 3). As expected, no differences in localization compared to FLAG-tagged M mutants in HEK-293T cells were monitored. Interestingly, for M variants that lacked PM targeting, we noted fluorescence emission also in the nucleus. Since mNeonGreen is found in the cytosol and nucleus when expressed alone, the intrinsic localization of mNeonGreen is likely dominant when attached to M protein variants lacking PM binding.

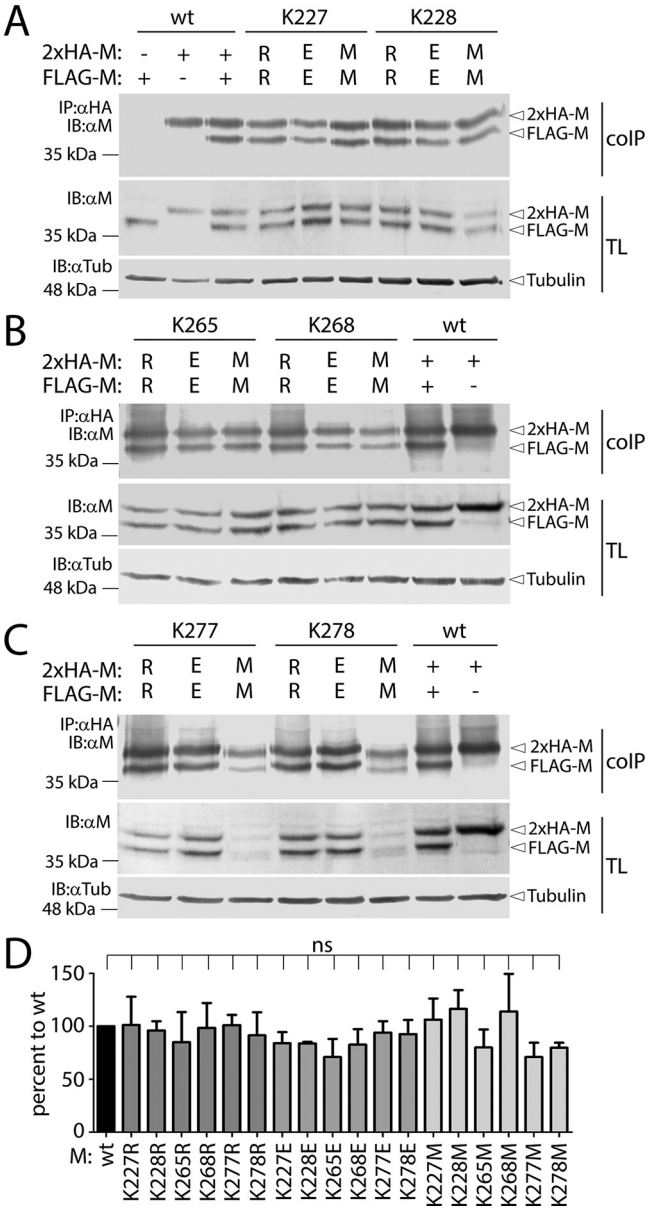

FIG 4 Investigation of self-assembly by coimmunoprecipitation (coIP). (A to C) The inherent self-assembly efficiencies of M wt and mutant proteins were determined by coIP and immunoblot (IB) analysis. The antibodies used for the immunoprecipitation (IP) and IB are indicated on the left (αHA, αM, and αTub). The different tagged mutants are labeled on the right and above, respectively. TL, total cell lysate. (D) The graphic shows the coIP efficiency index from three independent experiments (means and standard deviation [SD]). All ratios were normalized to wild-type M.

Nonconservative M protein lysine mutants retained self-assembly efficiency. To exclude the possibility that loss of PM targeting of selected M mutants was secondary to improper protein folding/assembly, coimmunoprecipitation (coIP) assays were carried out. In order to distinguish between IP and coIP M proteins in a single setting, HEK-293T cells were cotransfected with DNA plasmids encoding for M proteins of different sizes as follows: (i) a FLAG-linker-tagged M variant and (ii) a 2× hemagglutinin (HA) double-linker-tagged M mutant. Mixed M protein populations extracted from total cell lysates (TL) were immunoprecipitated using anti-HA monoclonal antibody (αHA) and fractionated in SDS-PAGE gels under reducing conditions. Upon membrane transfer, M proteins were finally detected using a polyclonal anti-M_{CDV} antibody (αM) (Fig. 4A to C). Regardless of the tag (FLAG or 2×HA), all M mutants were

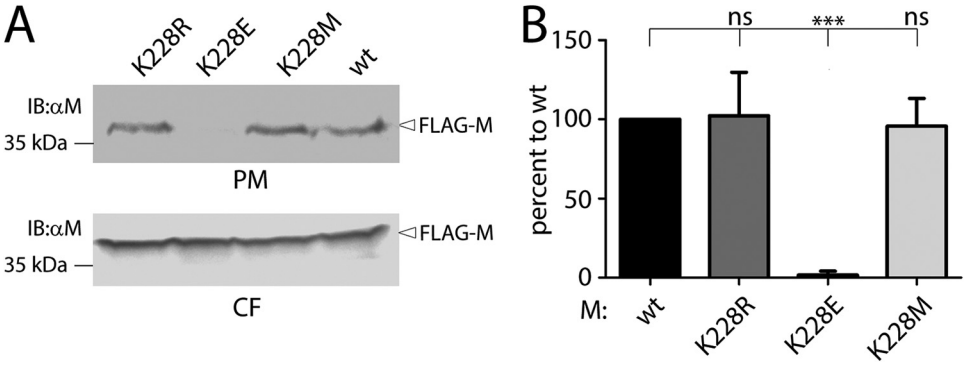

FIG 5 Analysis of plasma membrane association of various CDV M mutants. (A) The association of M-K228 mutants with the PM was analyzed using a plasma membrane protein extraction kit. The immunoblots show M wt and mutants either copurified with the PM or with cytosolic proteins (CF). The antibodies used for the IBs are shown on the left (αHA). (B) The graphic shows the ratios between the PM- and cytosolic-associated M proteins from three independent experiments (means and SD). All ratios were normalized to wild-type M.

expressed in cells, although M-K277M and -K278M exhibited limited expression profiles (Fig. 4C). As expected, when both protein variants were expressed separately, no coIP (FLAG-tagged) M proteins were detected (Fig. 4A). In contrast, (FLAG-tagged) M was readily pulled down in conditions where both M wt variants were coexpressed in the same cells, thereby validating our biochemical assay. Strikingly, all conservative, neutral, and nonconservative M variants preserved their ability to self-assemble. We also calculated the coIP efficiency index (ratio between the intensity of the IP and coIP M protein bands divided by the ratio of the TL M protein bands), which clearly confirmed that self-assembly remained mostly unaffected regardless of the amino acid side chain present at the selected M positions (Fig. 4D). Collectively, our data reveled that mutating lysine residues within CDV M-CTD did not significantly alter the overall M protein structural architecture.

We observed a minor shift in gel migration specifically for M-K277M and -K278M mutants, which is likely a consequence of the introduction of the hydrophobic side chain at those two specific positions, given that other amino acid modifications (R and E) did not lead to any obvious detectable difference (Fig. 4C).

The cytosolic retention profile of nonconservative M mutants correlates with lack of association with the plasma membrane. To determine whether the lack of cell periphery accumulation phenotype observed with nonconservative M mutants specifically correlated with deficiency in PM association, we processed some targeted mutants (M-K228) with a biochemical assay enabling focused analyses on the PM fraction. As expected, the M-K228R and M-K228M protein variants, which were characterized by intact cell periphery accumulation, also exhibited proper interaction with the lipids of the PM (Fig. 5). In sharp contrast, the M-K228E mutant, which was associated with cytosolic retention, was barely detected in the PM fraction (Fig. 5). In summary, these findings provided strong evidence that switching the negative charge at targeted lysine residues within CDV M-CTD prevented cell periphery targeting as a consequence of impaired association with the PM.

M mutants with PM targeting deficiencies also failed to produce VLPs. The delivery of CDV M to the cell surface, its arrangement into a regular lattice beneath the PM, and its association are considered to be essential for the production of M-induced VLPs. To investigate the inherent capacity of CDV M and its derivative mutants to release VLPs, we employed a previously described biochemical assay (59). The VLP budding index illustrates the ratio between the M signal derived from the cell supernatant (VLPs) versus the M signal recorded from the total cell lysate (TL) (Fig. 6). Conservative M lysine mutants, which preserved the PM binding capacity and were localized at the PM, remained functional in VLP formation (>50%) (Fig. 6A to C and E). Among the methionine mutants, only M-K227M and M-K228M remained partially

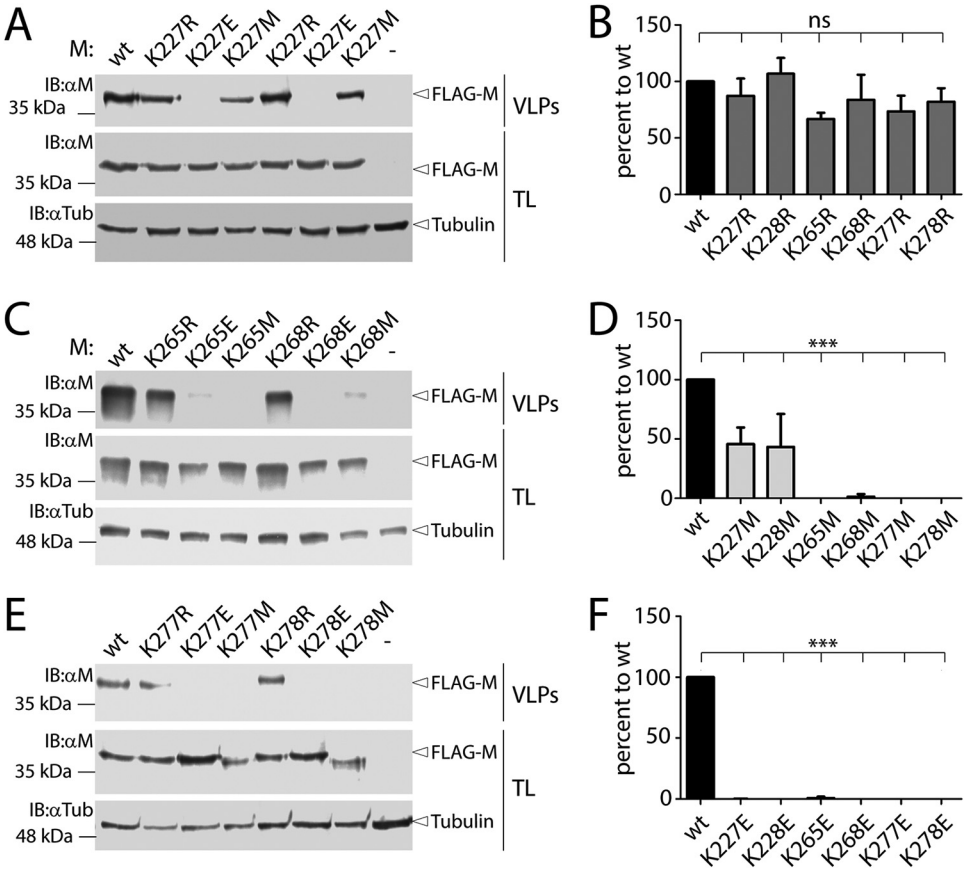

FIG 6 Analysis of VLP production induced by CDV M mutants. (A, C, E) VLPs were purified from the supernatants of HEK-293T cells expressing M mutants at 48 h posttransfection (hpt) by centrifugation through a 25% glycerol cushion. Equal amounts of total cell lysate (TL) and VLPs were subjected to SDS-PAGE and Western blotting analysis. The antibody used for the immunoblot is shown on the left (αM). As loading control, tubulin was detected thanks to a monoclonal anti-tubulin antibody (αTub). (A) K227/8-mutants, (C) K265/8-mutants, (E) K277/8-mutants. (B, D, F) The graphic represents the means and SD of the budding index, which was defined as the amount of M in the VLPs divided by the amount in TL from three independent experiments.

functional (VLP formed at ~50% compared to that of the wt) (Fig. 6A and D), correlating with their efficient PM targeting. Conversely, the intracellularly retained mutants M-K265M, M-K268M, M-K277M, and M-K278M were entirely defective in VLP formation (Fig. 6C to E). Finally, all tested nonconservative M mutants with a clear cytosolic phenotype secondary to lack of PM interactions were also drastically impaired in VLP production (Fig. 6A, C, E, and F). Altogether, these results confirmed and further expanded the mechanistic reach of our previous findings: the negative charge at selected lysine residues (positions 227, 228, 265, 268, 277, and 278) within M-CTD, while not crucial in protein folding, is essential in regulating PM localization/association and enabling productive membrane budding activity.

Lysine residue at position 238 of CDV M affects protein folding. The potentially mostly buried position of lysine residue 238 in the M protein was consistent with a different molecular mechanism leading to the lack of PM localization. To address this possibility, we submitted the M-K238 mutants to the coIP and VLP biochemical assays. Although M-K238R and M-K238M preserved their ability to efficiently oligomerize, we observed a low level of expression for the mutant M-K238E (and therefore any coIP M could be observed) since only barely detected in Western blotting analyses (Fig. 7A and B). Membrane budding activity was retained by M-K238R only, whereas M-K238E/M were strongly impaired in VLP production (Fig. 7C and D). Collectively, our results revealed that the M-K238E mutant was not expressed properly, which explained the

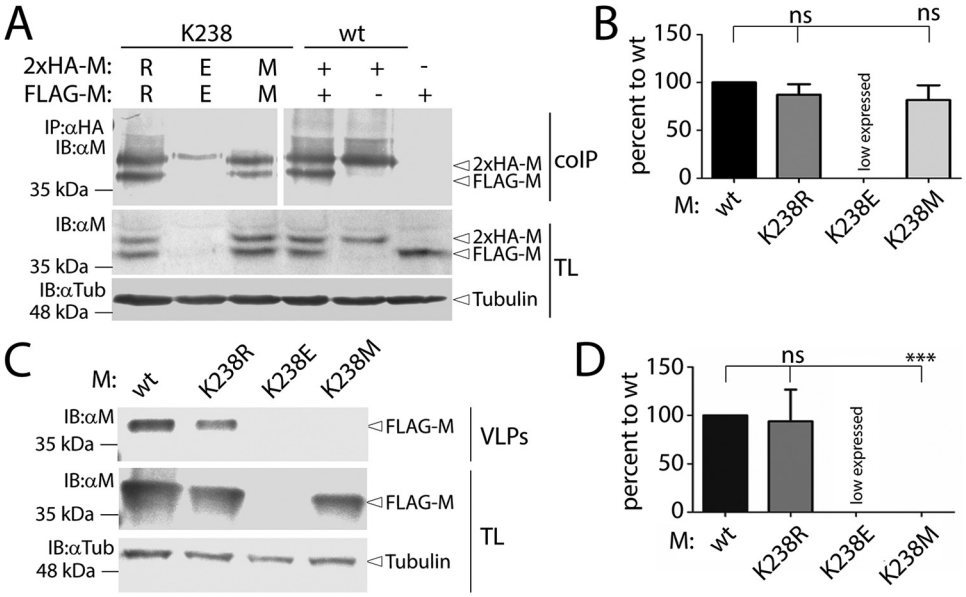

FIG 7 Investigation of K238 function. (A) The inherent self-assembly efficiencies of M-K238 mutants were determined by coIP and IB analysis. The antibodies used for the IP and IB are shown on the left (αHA, αM, and αTub). The different tagged mutants are labeled on the right and above, respectively. The white line indicates where the image was cropped for better presentation. (B) The graphic shows the coIP efficiency index from three independent experiments (means and SD). All ratios were normalized to wild-type M, which was arbitrarily set at 100%. (C) VLPs were purified from the supernatants of HEK-293T cells expressing M-K238 mutants at 48 hpt. Equal amounts of TL and VLPs were subjected to SDS-PAGE and Western blotting analysis. The antibody used for the immunoblot is indicated on the left (αM). As loading control, tubulin was revealed by employing a monoclonal anti-tubulin antibody (αTub). (D) The graphic represents the means and SD of the budding index, which was defined as the amount of M in the VLPs divided by the amount in cell lysates.

lack of PM targeting. This result strongly supported our initial hypothesis predicting the lysine residue at position 238 to be critical for protein folding.

Recombinant viruses bearing nonconservative mutation at selected M positions are defective in viral particle formation. We previously determined that some nonconservative M lysine mutants were defective in VLP formation. To study these mutations in a more biologically relevant context, we engineered three recombinant viruses: rA75/17-M-K227R, rA75/17-M-K227E, and rA75/17-M-K227M. Because budding-deficient viruses cannot be efficiently recovered from cDNA, we established a complementation system. In this set of experiments, we transiently coexpressed vesicular stomatitis virus (VSV)-G in addition to all other plasmids necessary for viral rescue. Indeed, the VSV-G glycoprotein not only drives cell entry but also contains the inherent ability to form VLPs. Using this strategy, we could successfully generate stock of infectious viruses harboring a defective M protein. Stocks of recombinant *trans*-complemented viruses were then transferred to Vero-cSLAM cells (~50 to 100 PFU), and the impact of the different M variants on membrane budding activity was assessed 3 days postinfection (determination of the infectivity titers from collected cell-associated [CA] and cell-free [SN] viruses).

While CA titers obtained from rA75/17-M-wt- and rA75/17-M-K227R-infected Vero-cSLAM cells reached a plateau at about 2.0×10^4 50% tissue culture infective dose ($TCID_{50}$)/ml (Fig. 8A), SN titers recorded for these two viruses peaked at 4.0×10^3 $TCID_{50}$/ml (Fig. 8B). In contrast, rA75/17-M-K227M showed reduced budding activity (~3.5×10^3 $TCID_{50}$/ml for CA and 1.4×10^2 $TCID_{50}$/ml for SN). Finally, the rA75/17M-K227E virus was markedly defective in infectious virus production (~1.7×10^1 $TCID_{50}$/ml for CA and SN). Altogether, these data confirmed the results obtained with the M protein-based VLP assay. Conservative M lysine mutants retained membrane budding activity (VLPs and infectious virus production), whereas nonconservative M lysine mutants did not. We also noted that, regardless of the M protein variant

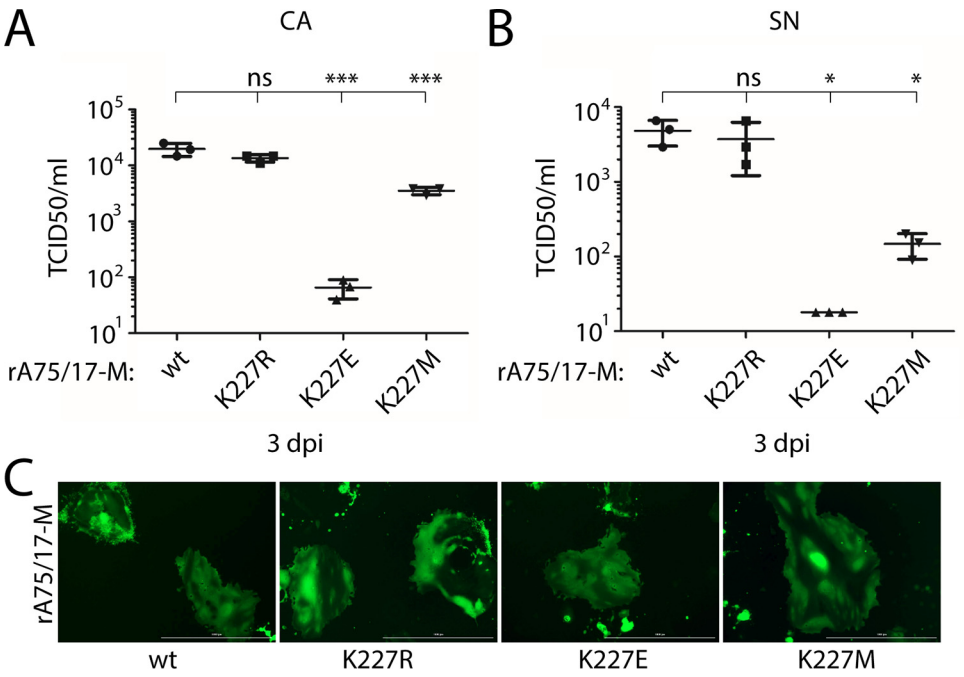

FIG 8 Analysis of progeny virus production of recombinant canine distemper virus bearing a single nonconservative mutation of the lysine within the M-CTD. Viral titers of rescued rA75/17 viruses containing M-wt, -K227R, -K227E, and -K227M mutants from three independent experiments are shown as follows: cell-associated (CA) progeny viruses (A) and cell-free (SN) progeny viruses (B). (C) Syncytia formation in Vero-cSLAM cells 3 days postinfection (dpi). Pictures of representative fields of view were acquired using an Invitrogen EVOS M5000 microscope.

expressed, all three viruses were efficiently triggering membrane fusion activity (Fig. 8C).

The proteasome inhibitor bortezomib reduces M-dependent VLP formation. It is assumed that multiple posttranslational modifications can target surface-exposed lysine residues of proteins (i.e., ubiquitination, SUMOylation, acetylation). Interestingly, several members of the families *Paramyxoviridae* and *Paramyxovirinae* encode matrix proteins that are indeed ubiquitinated, a posttranslational modification that may be acquired within the nucleus and important for controlling nuclear export, viral assembly, and egress (34, 35). However, although recent studies suggested that the morbillivirus M protein (including MeV and CDV) may not traffic through the nucleus (42), previous data nevertheless indicated efficient ubiquitination at lysine position 240 of the MeV M protein (34).

To investigate whether (i) CDV M is equally ubiquitinated and (ii) this posttranslational modification contributes to membrane budding activity, we took advantage of the drug bortezomib, a well-characterized FDA-approved proteasome inhibitor that leads to the depletion of free ubiquitin in the cell (35, 73). Strikingly, in bortezomib-treated cells, M wt was characterized by a dose-dependent reduction of VLP formation (Fig. 9A and B). Given that expression levels of exogenous (FLAG-M) and endogenous (tubulin) proteins in the total cell lysate were comparable to dimethyl sulfoxide (DMSO)-treated samples, we excluded cytotoxicity as the major cause of reduced VLP production in M-expressing cells. Moreover, M-driven membrane budding activity was partially restored by exogenous overexpression of a mutated ubiquitin version (HA-Ub-K0) (Fig. 9C and D). This ubiquitin variant contains all lysine residues replaced by arginines (74), which in turn leads to monoubiquitination of target proteins, a post-translational modification relevant to several regulatory functions. In summary, these results confirmed the essential role of the ubiquitination in CDV M-mediated VLP formation, even though the CDV M protein may not traffic through the nucleus like other paramyxovirus matrix proteins.

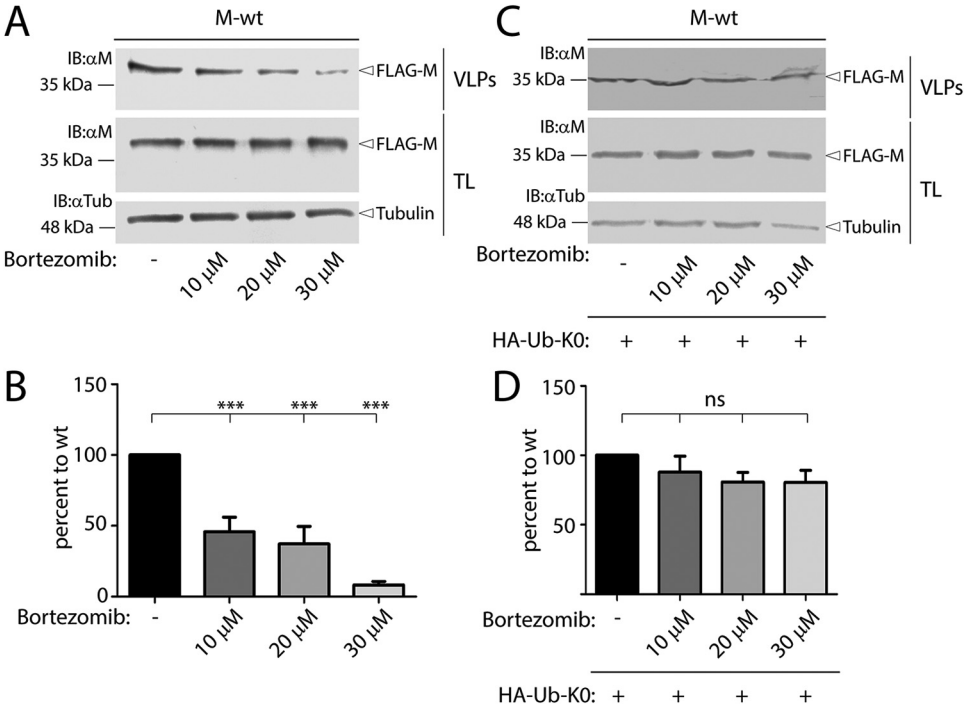

FIG 9 VLP formation of CDV M-wt in the presence of the proteasome inhibitor bortezomib. (A, C) CDV M-wt VLP budding in the presence of bortezomib. HEK-293T cells expressing FLAG-M-wt (A) or coexpressing FLAG-M-wt plus HA-Ub-K0 (C) were incubated with DMSO, 10 μM, 20 μM, or 30 μM bortezomib for 24 h. VLPs and cell lysates were immunoblotted with a polyclonal anti-M_{CDV} antibody (αM). As loading control, tubulin was revealed by employing a monoclonal anti-tubulin antibody (αTub). (B, D) The graphics represent the means and SD of the budding index, which was defined as the amount of M in the VLPs divided by the amount in cell lysates.

CDV M-CTD lysine mutants remain properly ubiquitinated. Given that the proteasome inhibitor bortezomib potently inhibited M-driven VLP formation, we next investigated whether the studied lysine residues within M-CTD were involved in ubiquitination. In order to biochemically determine the ubiquitination status of the various M mutants, we coexpressed FLAG-M with HA-Ub-K0 in HEK-293T cells. One day posttransfection (potentially ubiquitinated), M proteins were immunoprecipitated with a monoclonal anti-HA antibody and, upon Western blotting analyses, CDV M was detected using a polyclonal anti-M_{CDV} antibody. Regardless of whether the M lysine residues were mutated into conservative (Fig. 10A and B) or nonconservative amino acids (Fig. 10E and F), all M protein variants preserved wt-like monoubiquitination profiles. Remarkably, even dual M lysine mutants remained properly ubiquitinated (Fig. 10C and D). Collectively, these data not only demonstrate the importance of ubiquitination in M-mediated membrane budding activity but further suggest that additional lysine residues, besides that targeted in this study, are involved in this functionally essential posttranslational modification.

DISCUSSION

A recent cryo-electron tomography (cryo-ET) study of the measles virus matrix protein revealed evidence for a grid-like organization under both the plasma membrane (PM) of infected cells and the viral envelope (61). These findings were consistent with previous data obtained for related pneumoviruses and paramyxoviruses (i.e., NDV, RSV, HeV, hMPV), indicating a possible underlying conserved mechanism mediated by M proteins for membrane budding activity (27, 55–58). However, although cryo-ET analyses revealed interaction of MeV M with lipids, glycoproteins, and nucleocapsids, the limited structural resolution not only precluded the determination of the precise orientation of M within the network but could not highlight microdomains regulating functional interactions.

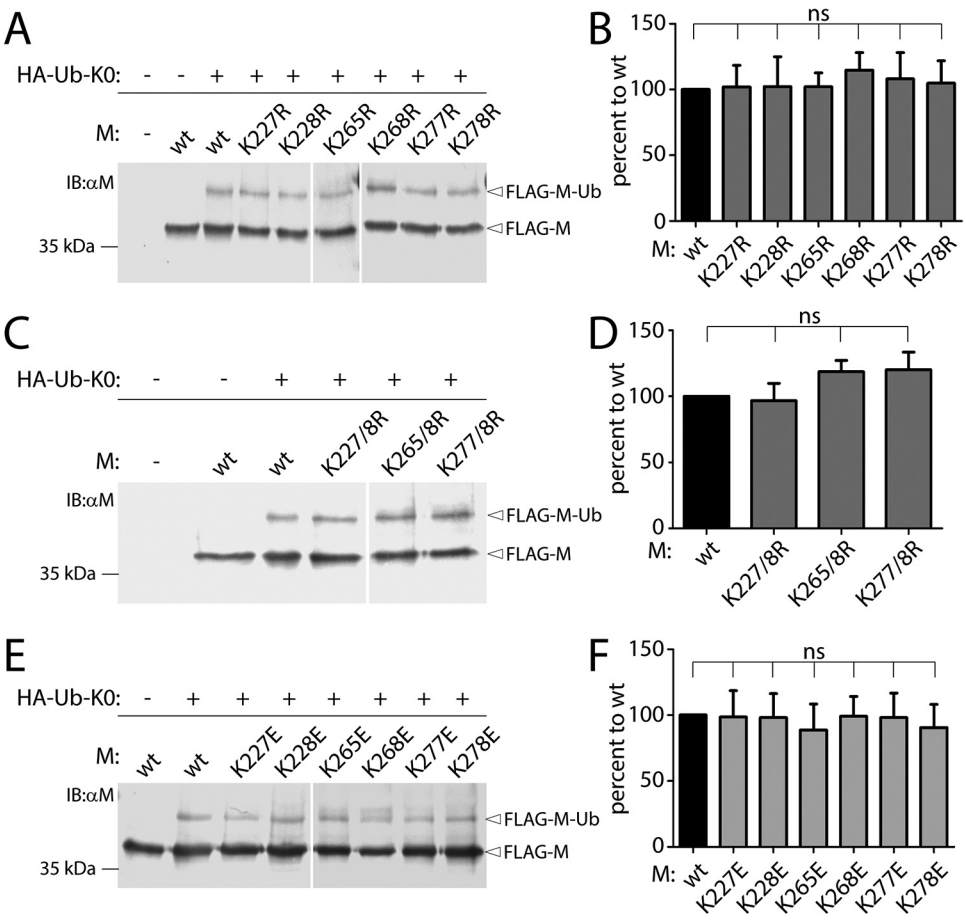

FIG 10 Ubiquitination of lysine residues within CTD of CDV M. (A, C, E) Immunoblot analysis of ubiquitination of lysine mutants of CDV M. HEK-293T cells were cotransfected with HA-Ub-K0 and the FLAG-tagged M-wt or indicated mutant. Single R mutants (A), double R mutants (C), single E mutants (E). After 24 hpt, FLAG-tagged M was immunoprecipitated, and its ubiquitinated species were detected by Western blotting analysis using a polyclonal anti-MCDV antibody (αM). The white lines indicate where the images were cropped for better presentation. (B, D, F) The graphics represent the means and SD of the ubiquitination efficiency index, which was defined as the ratio of FLAG-M-Ub to FLAG-M. All ratios were normalized to wild-type M.

In some related paramyxoviral and filoviral viruses, large positively charged patches of matrix-like proteins were suggested to be involved in membrane association (3, 26–28, 63, 65, 70–72). Based on a homology 3D model, we highlighted two conserved, surface-exposed, basic patches, located within each CDV M-CTD protomer. Assuming the basic patch positioned toward the PM, part of the CTD might interact with the inner leaflet of the lipid bilayer, whereas other regions located within the NTD may point toward the cytosol and, upon budding, toward the inside of the viral particle. Such M orientation infers an interaction with nucleocapsids through the NTD and assembly of M oligomers as well as binding to the inner leaflet of lipid bilayers through the CTD. In this study, we aimed at providing biochemical and mechanistic evidence that CDV M-CTD (i) indeed contributes to PM binding and (ii) whether the binding relies on electrostatic interactions.

Toward this goal, nine lysine (K) residues encompassed within the M-CTD basic patch were mutated into alternative basic (R), neutral (M), and acidic (E) amino acids. Abrogation of PM association and release of VLPs in the supernatant with most of the nonconservative M mutants (K227E, K228E, K265E, K268E, K277E, and K278E), combined with the absence of any other large and uniform basic patches present on the surface of our CDV M structural model, provided strong evidence that the basic patch very likely interacted with the negatively charged inner leaflet of cellular membranes

(including the PM). Strikingly, switching a single positive charge of the large basic patch into a negative one was sufficient to severely impair M-mediated membrane association and release of VLPs. Importantly, these data are relevant for the whole infectious virus, since a recombinant CDV carrying the single M-K227E mutation also exhibited strong deficiency in virus progeny production. Although we cannot exclude that the introduced substitutions led to local conformational changes preventing membrane association, our data (indicating proper expression and self-assembly profiles of the nonconservative M mutants [except K238E]) led us to hypothesize that the basic patch promoted M-mediated electrostatic membrane interactions. Interestingly, while M mutants harboring a neutral amino acid (M) at positions 227 and 228 within the basic patch preserved PM targeting and partial membrane budding activity, M variants K265M, K268M, K277M, and K278M were completely deficient in promoting both functions. These data are consistent with lysine residues at position 265, 268, 277, and 278 of CDV M as key regulators of PM association and critical for membrane budding activity. Furthermore, the findings that recombinant viruses harboring nonconservative M mutants were drastically impaired in membrane budding activity, while still able to induce cell-cell fusion, demonstrated that the two expressed surface glycoproteins (H and F) could not restore egress of the recombinant viruses. These data further highlighted the essential role of M (and associated functions) and the identified lysines in viral budding activity.

Intriguingly, the M-K240E and M-K243E single mutants preserved plasma membrane localization, albeit displaying a negative charge within the basic patch. Based on our homology, the 3D structural model, and the proposed M orientation, K240 and K243 may not be ideally exposed toward the PM but may be located more sideway in the α9-helix; a microdomain hypothesized to contribute to M dimer-dimer contacts. Therefore, our data suggested that both lysines may not directly contribute to electrostatic interactions with lipids but would affect the assembly of M proteins into higher oligomers. Conversely, the structural model indicated that the nearby lysine residue at position 238 is only poorly exposed on the M protein surface. The limited expression profile monitored when this position was converted into a nonconserved amino acid (M-K238E) not only argued in favor of a role of this lysine residue in proper protein folding but strengthened the relevance of our 3D model. Consistently, mutating lysine 238 into an amino acid with a similar charge (R) led to M protein variants exhibiting wt-like phenotypes (PM targeting and VLP production). Interestingly, immunofluorescence analyses of M-K238M revealed that, despite a clear PM localization phenotype, the latter mutant was defective in VLP formation. For all other tested methionine mutants, PM targeting correlated with efficient VLP formation. Therefore, these results strongly supported our initial hypothesis, predicting the lysine residue at position 238 to be critical for protein folding. Replacing lysine 238 with an amino acid containing either a negative charge or a hydrophobic side chain may impact the overall structural M architecture and, consequently, compromise its multiple functions.

It was previously reported that some paramyxovirus and pneumovirus matrix proteins (i.e., SeV, NDV, RSV, NiV, HeV, and MuV) traffic through the nucleus via a conserved functional bipartite nuclear localization signal (NLS_{bp}) and, consequently, undergo ubiquitination, a posttranslational modification considered essential for controlling nuclear export, viral assembly, and membrane egress (34, 35). In sharp contrast, it was shown that CDV and MeV M proteins do not traffic through the nucleus (42), although ubiquitination at lysine residue 240 of the MeV M protein (K240) was proposed (34). Here, we provided evidence that the CDV M protein is equally ubiquitinated and that this modification was essential for M-mediated membrane budding activity. Indeed, in bortezomib-treated cells, CDV M lost its inherent ability to bud VLPs. Even though these findings suggested that ubiquitination of the morbillivirus matrix protein may be acquired in the cytosol, none of the analyzed CDV M lysine mutants (including those lacking electrostatic membrane interactions) exhibited substantial reduction of their ubiquitination profiles, which argued for alternative lysine residues regulating this essential process. Therefore, additional work is warranted to (i) identify which amino

acid(s) of the CDV M protein is important for ubiquitination and whether differences exist among morbilliviral members, (ii) determine the precise role of ubiquitinated M proteins in the morbilliviral life cycle, and (iii) define how ubiquitinated M proteins are arranged within the grid-like structure. Nevertheless, our findings provided further evidence for a crucial role of this posttranslational modification in regulating paramyxovirus and pneumovirus membrane egress.

In summary, our data identified multiple surface-exposed lysine residues located within the CTD of the CDV M protein, which critically contributed to PM association and ensuing membrane budding activity but were not involved in ubiquitination modifications. These findings provide novel mechanistic information on the largely unexplored multiple functions promoted by morbilliviral M proteins.

MATERIALS AND METHODS

Cell cultures and transfection. Depending on the experiment, the cells used included HEK-293T cells (ATCC CRL-11268), Vero cells stably expressing canine SLAM (Vero-cSLAM; kindly provided by Yusuke Yanagi, Kyushu University, Japan), BSR-T7 (75), and MDCK cells (ATCC CCL-34). Cells of every type were grown in Dulbecco's modified Eagle medium (DMEM; Gibco, Invitrogen) containing 10% fetal calf serum (FCS; Bioswisstech) and penicillin-streptomycin at 37°C in a 5% CO_2 atmosphere. Cells were transfected with TransIT-LT1 (Mirus) or Helix-IN (OZ Biosciences) by following the manufacturer's instructions.

Plasmids and mutagenesis. All mutant CDV M protein-expressing plasmids were based on the pCI vector containing CDV M of the A75/17 CDV strain (59). All CDV M variants had an N-terminal tag (FLAG, 2×HA, or the green fluorescent protein mNeonGreen). CDV mutations were introduced using In-Fusion HD cloning plus (Takara). Mutagenesis primer sequences will be communicated upon request.

Indirect immunofluorescence analysis. HEK-293T cells transfected with plasmids encoding CDV-M wt or mutants were fixed 24 h posttransfection (hpt) with 4% paraformaldehyde (PFA; pH 7.4) in phosphate-buffered saline (1× PBS) and permeabilized with 0.5% Triton X-100 in PBS. Immunodetection was performed using as a primary antibody mouse monoclonal anti-FLAG M2 antibody (1:1,000; Sigma-Aldrich) for FLAG-M constructs and rabbit monoclonal anti-sodium potassium ATPase antibody (1:500; Abcam) for the plasma membrane; as a secondary antibody, Alexa Fluor 555-conjuated goat anti-mouse IgG (H+L) and Alexa Fluor 488-conjugated goat anti-rabbit IgG (H+L) (1:1,000; Life Technologies) were used. Nuclei are counterstained with 4′,6-diamidino-2-phenylidole (DAPI; 1:5,000; AppliChem). Pictures were acquired by laser scanning confocal microscopy using Olympus FV3000 with FluoView FV3000 system software.

Fluorescence analysis of mNeonGreen-M constructs. MDCK cells were transfected with plasmids encoding CDV mNeonGreen-tagged M wt or mutants with Helix-IN (OZ Biosciences) by following the manufacturer's instructions. One day posttransfection, cells were fixed with 4% PFA (pH 7.4) in 1× PBS. Nuclei were counterstained with DAPI (1:5,000; AppliChem). Pictures were acquired by laser scanning confocal microscopy using Olympus FV3000 with FluoView FV3000 system software.

Western blotting. Western blotting and SDS-PAGE were performed with standard protocol. Samples were loaded onto 12% Tris-glycine SDS-PAGE. Separated proteins were transferred to nitrocellulose membranes (GE Healthcare Amersham protran premium 0.2-μm NC nitrocellulose membranes; Fisher) by electroblotting. Proteins were detected with an in-house-generated rabbit polyclonal anti-M_{CDV} antibody (αM) (1:1,000) (45) and a horseradish peroxidase (HRP)-conjugated goat anti-rabbit antibody (1:10,000; Dako) or a mouse monoclonal anti-tubulin antibody (αTub) (1:5,000; Abcam) and an HRP-conjugated rabbit anti-mouse antibody (1:5,000; Abcam). Chemiluminescence signals were detected using 1-Step Ultra TMB (3,3′,5,5′-tetramethylbenzidine)-blotting solution (Thermo Fisher Scientific) according to the manufacturer's instructions.

Production of viral-like particles. HEK-293T cells in 6-well plates were transfected with 3 μg per well of FLAG-tagged CDV-M or M mutants expressing constructs. Forty-eight hours posttransfection, 1 ml of the culture supernatants was collected and centrifuged (10 min; 500 × *g*; 4°C) to remove cellular debris. The clarified supernatants were incubated with 40 μl of 10× trypsin-EDTA solution (Sigma-Aldrich) for 30 min at 37°C. Subsequently, 50 μl of soybean trypsin inhibitor (1 mg/ml solved in distilled water; Roche Diagnostics) was added to reduce the activity of trypsin. Consequently, the supernatant mixtures were loaded on a 25% glycerol cushion and centrifuged at 16,100 × *g* for 2 h at 4°C. Following this, the supernatants mixture was removed, the VLP-pellets were resuspended in 0.2 M dithiothreitol (DTT)-1.6× Laemmli buffer (Bio-Rad), boiled at 97°C, and subjected to Western blotting analysis. As for the cell lysate expressions, cells were harvested in 1 ml PBS 48 hpt. A total of 100 μl of the cells were transferred in new tube and centrifuged (10 min; 500 × *g*; 4°C). The TL pellets were resuspended in 0.2 M DTT-1.6× Laemmli buffer (Bio-Rad), boiled at 97°C, and subjected to Western blotting analysis as described above. The intensities of the bands were quantified with the FUSION FX software (Vilber). The budding index was defined as the amount of M in the VLPs divided by the amount in TLs $\left(\frac{\text{VLP FLAG}-\text{M}}{\text{TL FLAG}-\text{M}}\right)$. All ratios were normalized to wild-type M, which was arbitrarily set at 100%.

Coimmunoprecipitation and immunoprecipitation of matrix ubiquitination. HEK-293T cells coexpressing FLAG-linker-M and 2×HA-double-linker-M, both bearing the same mutations, or coexpressing FLAG-linker-M variants and HA-ubiquitin-K0, were resuspended in PBS 24 hpt and centrifuged (10

min; 500 × *g*; 4°C). The cell pellets were lysed with radioimmunoprecipitation assay (RIPA) buffer (50 mM Tris, pH 7.2, 150 mM NaCl, 10 mM EDTA, 1% sodium deoxycholate, 1% Nonidet P-40, 0.05% SDS) containing protease inhibitor (Roche; cOmplete mix) for 1 h at 4°C. Cell lysates were clarified by centrifugation (16,100 × *g*; 20 min; 4°C). Supernatants were transferred into new tubes, and 15 μl of Dynabeads protein G (Invitrogen) were added as well as 1:1,000 monoclonal mouse anti-HA antibody (BioLegend) for coIP assay or 1:1,000 monoclonal mouse anti-FLAG M2 antibody (Sigma-Aldrich) for IP of matrix ubiquitination. The mixture was incubated overnight at 4°C on a rotating wheel. The beads were washed with PBS containing 0.05% Tween 20 (Merck), resuspended in 2× Laemmli buffer (Sigma-Aldrich), boiled at 97°C, and subjected to Western blotting analysis. The intensities of the bands were quantified with the FUSION FX software (Vilber). The coIP efficiency index was defined as the ratio of coIP to IP signals divided by the ratio of TLs as follows:

$$\left(\frac{\text{IP FLAG} - \text{M}}{\text{coIP2} \times \text{HA} - \text{M}} \Big/ \frac{\text{TL FLAG} - \text{M}}{\text{TL2} \times \text{HA} - \text{M}}\right)$$

The ubiquitination efficiency index was defined as the ratio of FLAG-M-Ub to FLAG-M $\left(\frac{\text{FLAG}-\text{M}-\text{Ub}}{\text{FLAG}-\text{M}}\right)$. All ratios were normalized to wild-type M, which was arbitrarily set at 100%.

Plasma membrane association. The association of M mutants with the plasma membrane was analyzed at 24 hpt using a plasma membrane protein extraction kit (101Bio) according to the manufacturer's protocol. The extracted plasma membrane- and cytosolic-associated proteins were resuspended in 2× Laemmli buffer (Sigma-Aldrich), boiled at 97°C, and subjected to Western blotting analysis.

Recombinant virus rescue. For the rescue of rA75/17-M-wt or -mutants, BSR-T7 cells were transfected with recombinant plasmids encoding the anti-genome along with helper plasmids (pMD2.G [Addgene], pTM-NOP$_{CDV}$, pTM-POP$_{CDV}$–Cko, pTM-LOP$_{CDV}$–V13E [unpublished data]) using TransIT-LT1 (Mirus) according to manufacturer's instructions. The cells were heat-shocked for 2 h at 42°C after 3 hpt, medium changed, and incubated for 48 h. Cells and supernatants were collected and frozen at −80°C overnight. Cells and supernatants were thawed and directly centrifuged (5 min, 800 × *g*, 4°C). Six-well plates were prepared with 0.7×10^6 Vero-cSLAM cells and infected with the supernatants for 72 h. Supernatant and cells were collected separately from the rescue for quantification of viral titers.

Statistical analysis. Statistical significance was determined using one-way analysis of variance (ANOVA) followed by Tukey's test using GraphPad Prism 5 to analyze differences between wild-type and mutant means (*, $P < 0.05$; ***, $P < 0.001$; ns: not significant).

ACKNOWLEDGMENT

This work was supported by the Swiss National Science Foundation (refs. no. 310030_173185 to P.P.).

REFERENCES

1. Amarasinghe GK, Ayllón MA, Bào Y, Basler CF, Bavari S, Blasdell KR, Briese T, Brown PA, Bukreyev A, Balkema-Buschmann A, Buchholz UJ, Chabi-Jesus C, Chandran K, Chiapponi C, Crozier I, de Swart RL, Dietzgen RG, Dolnik O, Drexler JF, Dürrwald R, Dundon WG, Duprex WP, Dye JM, Easton AJ, Fooks AR, Formenty PBH, Fouchier RAM, Freitas-Astúa J, Griffiths A, Hewson R, Horie M, Hyndman TH, Jiāng D, Kitajima EW, Kobinger GP, Kondō H, Kurath G, Kuzmin IV, Lamb RA, Lavazza A, Lee B, Lelli D, Leroy EM, Lǐ J, Maes P, Marzano S-YL, Moreno A, Mühlberger E, Netesov SV, Nowotny N, et al. 2019. Taxonomy of the order Mononegavirales: update 2019. Arch Virol 164:1967–1980. https://doi.org/10.1007/s00705-019-04247-4.
2. Rima B, Balkema-Buschmann A, Dundon WG, Duprex P, Easton A, Fouchier R, Kurath G, Lamb R, Lee B, Rota P, Wang L, ICTV Report Consortium. 2019. ICTV virus taxonomy profile: Paramyxoviridae. J Gen Virol 100:1593–1594. https://doi.org/10.1099/jgv.0.001328.
3. Lamb RA, Parks GD. 2013. Paramyxoviridae: the viruses and their replication, p 957–995. *In* Knipe DM, Howley PM (ed), Fields virology. Lippincott Williams & Wilkins, Philadelphia, PA.
4. Ader-Ebert N, Khosravi M, Herren M, Avila M, Alves L, Bringolf F, Orvell C, Langedijk JP, Zurbriggen A, Plemper RK, Plattet P. 2015. Sequential conformational changes in the morbillivirus attachment protein initiate the membrane fusion process. PLoS Pathog 11:e1004880. https://doi.org/10.1371/journal.ppat.1004880.
5. Ader N, Brindley MA, Avila M, Origgi FC, Langedijk JP, Orvell C, Vandevelde M, Zurbriggen A, Plemper RK, Plattet P. 2012. Structural rearrangements of the central region of the morbillivirus attachment protein stalk domain trigger F protein refolding for membrane fusion. J Biol Chem 287:16324–16334. https://doi.org/10.1074/jbc.M112.342493.
6. Apte-Sengupta S, Navaratnarajah CK, Cattaneo R. 2013. Hydrophobic and charged residues in the central segment of the measles virus hemagglutinin stalk mediate transmission of the fusion-triggering signal. J Virol 87:10401–10404. https://doi.org/10.1128/JVI.01547-13.
7. Brindley MA, Takeda M, Plattet P, Plemper RK. 2012. Triggering the measles virus membrane fusion machinery. Proc Natl Acad Sci U S A 109:E3018–E3027. https://doi.org/10.1073/pnas.1210925109.
8. Herren M, Shrestha N, Wyss M, Zurbriggen A, Plattet P. 2018. Regulatory role of the morbillivirus attachment protein head-to-stalk linker module in membrane fusion triggering. J Virol 92:e00679-18. https://doi.org/10.1128/JVI.00679-18.
9. Plattet P, Alves L, Herren M, Aguilar HC. 2016. Measles virus fusion protein: structure, function and inhibition. Viruses 8:112. https://doi.org/10.3390/v8040112.
10. Navaratnarajah CK, Negi S, Braun W, Cattaneo R. 2012. Membrane fusion triggering: three modules with different structure and function in the upper half of the measles virus attachment protein stalk. J Biol Chem 287:38543–38551. https://doi.org/10.1074/jbc.M112.410563.
11. Navaratnarajah CK, Kumar S, Generous A, Apte-Sengupta S, Mateo M, Cattaneo R. 2014. The measles virus hemagglutinin stalk: structures and functions of the central fusion activation and membrane-proximal segments. J Virol 88:6158–6167. https://doi.org/10.1128/JVI.02846-13.
12. Russell CJ, Jardetzky TS, Lamb RA. 2001. Membrane fusion machines of paramyxoviruses: capture of intermediates of fusion. EMBO J 20:4024–4034. https://doi.org/10.1093/emboj/20.15.4024.
13. Plattet P, Plemper RK. 2013. Envelope protein dynamics in paramyxovirus entry. mBio 4:e00413-13. https://doi.org/10.1128/mBio.00413-13.
14. Bose S, Jardetzky TS, Lamb RA. 2015. Timing is everything: fine-tuned molecular machines orchestrate paramyxovirus entry. Virology 479–480:518–531. https://doi.org/10.1016/j.virol.2015.02.037.
15. Tatsuo H, Ono N, Tanaka K, Yanagi Y. 2000. SLAM (CDw150) is a cellular

receptor for measles virus. Nature 406:893–897. https://doi.org/10.1038/35022579.
16. Baron MD. 2005. Wild-type rinderpest virus uses SLAM (CD150) as its receptor. J Gen Virol 86:1753–1757. https://doi.org/10.1099/vir.0.80836-0.
17. Tatsuo H, Ono N, Yanagi Y. 2001. Morbilliviruses use signaling lymphocyte activation molecules (CD150) as cellular receptors. J Virol 75:5842–5850. https://doi.org/10.1128/JVI.75.13.5842-5850.2001.
18. Birch J, Juleff N, Heaton MP, Kalbfleisch T, Kijas J, Bailey D. 2013. Characterization of ovine nectin-4, a novel peste des petits ruminants virus receptor. J Virol 87:4756–4761. https://doi.org/10.1128/JVI.02792-12.
19. Noyce RS, Delpeut S, Richardson CD. 2013. Dog nectin-4 is an epithelial cell receptor for canine distemper virus that facilitates virus entry and syncytia formation. Virology 436:210–220. https://doi.org/10.1016/j.virol.2012.11.011.
20. Noyce RS, Richardson CD. 2012. Nectin 4 is the epithelial cell receptor for measles virus. Trends Microbiol 20:429–439. https://doi.org/10.1016/j.tim.2012.05.006.
21. Zhang X, Lu G, Qi J, Li Y, He Y, Xu X, Shi J, Zhang CW, Yan J, Gao GF. 2013. Structure of measles virus hemagglutinin bound to its epithelial receptor nectin-4. Nat Struct Mol Biol 20:67–72. https://doi.org/10.1038/nsmb.2432.
22. Muhlebach MD, Mateo M, Sinn PL, Prufer S, Uhlig KM, Leonard VH, Navaratnarajah CK, Frenzke M, Wong XX, Sawatsky B, Ramachandran S, McCray PB, Jr, Cichutek K, von Messling V, Lopez M, Cattaneo R. 2011. Adherens junction protein nectin-4 is the epithelial receptor for measles virus. Nature 480:530–533. https://doi.org/10.1038/nature10639.
23. Pratakpiriya W, Seki F, Otsuki N, Sakai K, Fukuhara H, Katamoto H, Hirai T, Maenaka K, Techangamsuwan S, Lan NT, Takeda M, Yamaguchi R. 2012. Nectin4 is an epithelial cell receptor for canine distemper virus and involved in neurovirulence. J Virol 86:10207–10210. https://doi.org/10.1128/JVI.00824-12.
24. Zipperle L, Langedijk JP, Orvell C, Vandevelde M, Zurbriggen A, Plattet P. 2010. Identification of key residues in virulent canine distemper virus hemagglutinin that control CD150/SLAM-binding activity. J Virol 84:9618–9624. https://doi.org/10.1128/JVI.01077-10.
25. Takimoto T, Portner A. 2004. Molecular mechanism of paramyxovirus budding. Virus Res 106:133–145. https://doi.org/10.1016/j.virusres.2004.08.010.
26. Harrison MS, Sakaguchi T, Schmitt AP. 2010. Paramyxovirus assembly and budding: building particles that transmit infections. Int J Biochem Cell Biol 42:1416–1429. https://doi.org/10.1016/j.biocel.2010.04.005.
27. Battisti AJ, Meng G, Winkler DC, McGinnes LW, Plevka P, Steven AC, Morrison TG, Rossmann MG. 2012. Structure and assembly of a paramyxovirus matrix protein. Proc Natl Acad Sci U S A 109:13996–14000. https://doi.org/10.1073/pnas.1210275109.
28. Cox RM, Plemper RK. 2017. Structure and organization of paramyxovirus particles. Curr Opin Virol 24:105–114. https://doi.org/10.1016/j.coviro.2017.05.004.
29. Takimoto T, Murti KG, Bousse T, Scroggs RA, Portner A. 2001. Role of matrix and fusion proteins in budding of Sendai virus. J Virol 75:11384–11391. https://doi.org/10.1128/JVI.75.23.11384-11391.2001.
30. Sugahara F, Uchiyama T, Watanabe H, Shimazu Y, Kuwayama M, Fujii Y, Kiyotani K, Adachi A, Kohno N, Yoshida T, Sakaguchi T. 2004. Paramyxovirus Sendai virus-like particle formation by expression of multiple viral proteins and acceleration of its release by C protein. Virology 325:1–10. https://doi.org/10.1016/j.virol.2004.04.019.
31. Pohl C, Duprex WP, Krohne G, Rima BK, Schneider-Schaulies S. 2007. Measles virus M and F proteins associate with detergent-resistant membrane fractions and promote formation of virus-like particles. J Gen Virol 88:1243–1250. https://doi.org/10.1099/vir.0.82578-0.
32. Patch JR, Crameri G, Wang LF, Eaton BT, Broder CC. 2007. Quantitative analysis of Nipah virus proteins released as virus-like particles reveals central role for the matrix protein. Virol J 4:1. https://doi.org/10.1186/1743-422X-4-1.
33. Cathomen T, Mrkic B, Spehner D, Drillien R, Naef R, Pavlovic J, Aguzzi A, Billeter MA, Cattaneo R. 1998. A matrix-less measles virus is infectious and elicits extensive cell fusion: consequences for propagation in the brain. EMBO J 17:3899–3908. https://doi.org/10.1093/emboj/17.14.3899.
34. Pentecost M, Vashisht AA, Lester T, Voros T, Beaty SM, Park A, Wang YE, Yun TE, Freiberg AN, Wohlschlegel JA, Lee B. 2015. Evidence for ubiquitin-regulated nuclear and subnuclear trafficking among Paramyxovirinae matrix proteins. PLoS Pathog 11:e1004739. https://doi.org/10.1371/journal.ppat.1004739.
35. Wang YE, Park A, Lake M, Pentecost M, Torres B, Yun TE, Wolf MC, Holbrook MR, Freiberg AN, Lee B. 2010. Ubiquitin-regulated nuclear-cytoplasmic trafficking of the Nipah virus matrix protein is important for viral budding. PLoS Pathog 6:e1001186. https://doi.org/10.1371/journal.ppat.1001186.
36. Coleman NA, Peeples ME. 1993. The matrix protein of Newcastle disease virus localizes to the nucleus via a bipartite nuclear localization signal. Virology 195:596–607. https://doi.org/10.1006/viro.1993.1411.
37. Ghildyal R, Ho A, Dias M, Soegiyono L, Bardin PG, Tran KC, Teng MN, Jans DA. 2009. The respiratory syncytial virus matrix protein possesses a Crm1-mediated nuclear export mechanism. J Virol 83:5353–5362. https://doi.org/10.1128/JVI.02374-08.
38. Ghildyal R, Ho A, Wagstaff KM, Dias MM, Barton CL, Jans P, Bardin P, Jans DA. 2005. Nuclear import of the respiratory syncytial virus matrix protein is mediated by importin β1 independent of importin alpha. Biochemistry 44:12887–12895. https://doi.org/10.1021/bi050701e.
39. Duan Z, Li Q, He L, Zhao G, Chen J, Hu S, Liu X. 2013. Application of green fluorescent protein-labeled assay for the study of subcellular localization of Newcastle disease virus matrix protein. J Virol Methods 194:118–122. https://doi.org/10.1016/j.jviromet.2013.08.014.
40. Peeples ME, Wang C, Gupta KC, Coleman N. 1992. Nuclear entry and nucleolar localization of the Newcastle disease virus (NDV) matrix protein occur early in infection and do not require other NDV proteins. J Virol 66:3263–3269. https://doi.org/10.1128/JVI.66.5.3263-3269.1992.
41. Bauer A, Neumann S, Karger A, Henning AK, Maisner A, Lamp B, Dietzel E, Kwasnitschka L, Balkema-Buschmann A, Keil GM, Finke S. 2014. ANP32B is a nuclear target of henipavirus M proteins. PLoS One 9:e97233. https://doi.org/10.1371/journal.pone.0097233.
42. Gunther M, Bauer A, Muller M, Zaeck L, Finke S. 2020. Interaction of host cellular factor ANP32B with matrix proteins of different paramyxoviruses. J Gen Virol 101:44–58. https://doi.org/10.1099/jgv.0.001362.
43. Iwasaki M, Takeda M, Shirogane Y, Nakatsu Y, Nakamura T, Yanagi Y. 2009. The matrix protein of measles virus regulates viral RNA synthesis and assembly by interacting with the nucleocapsid protein. J Virol 83:10374–10383. https://doi.org/10.1128/JVI.01056-09.
44. Wakimoto H, Shimodo M, Satoh Y, Kitagawa Y, Takeuchi K, Gotoh B, Itoh M. 2013. F-actin modulates measles virus cell-cell fusion and assembly by altering the interaction between the matrix protein and the cytoplasmic tail of hemagglutinin. J Virol 87:1974–1984. https://doi.org/10.1128/JVI.02371-12.
45. Wiener D, Plattet P, Cherpillod P, Zipperle L, Doherr MG, Vandevelde M, Zurbriggen A. 2007. Synergistic inhibition in cell-cell fusion mediated by the matrix and nucleocapsid protein of canine distemper virus. Virus Res 129:145–154. https://doi.org/10.1016/j.virusres.2007.07.004.
46. Mahapatra M, Parida S, Baron MD, Barrett T. 2006. Matrix protein and glycoproteins F and H of Peste-des-petits-ruminants virus function better as a homologous complex. J Gen Virol 87:2021–2029. https://doi.org/10.1099/vir.0.81721-0.
47. Dietzel E, Kolesnikova L, Maisner A. 2013. Actin filaments disruption and stabilization affect measles virus maturation by different mechanisms. Virol J 10:249. https://doi.org/10.1186/1743-422X-10-249.
48. Klauschies F, Gutzkow T, Hinkelmann S, von Messling V, Vaske B, Herrler G, Haas L. 2010. Viral infectivity and intracellular distribution of matrix (M) protein of canine distemper virus are affected by actin filaments. Arch Virol 155:1503–1508. https://doi.org/10.1007/s00705-010-0737-6.
49. Katayama H, Hori M, Sato K, Kajita M, Ozaki H, Karaki H, Ohashi K, Kai C. 2004. Role of actin microfilaments in canine distemper virus replication in Vero cells. J Vet Med Sci 66:409–415. https://doi.org/10.1292/jvms.66.409.
50. Runkler N, Pohl C, Schneider-Schaulies S, Klenk HD, Maisner A. 2007. Measles virus nucleocapsid transport to the plasma membrane requires stable expression and surface accumulation of the viral matrix protein. Cell Microbiol 9:1203–1214. https://doi.org/10.1111/j.1462-5822.2006.00860.x.
51. Riedl P, Moll M, Klenk HD, Maisner A. 2002. Measles virus matrix protein is not cotransported with the viral glycoproteins but requires virus infection for efficient surface targeting. Virus Res 83:1–12. https://doi.org/10.1016/S0168-1702(01)00379-3.
52. Naim HY, Ehler E, Billeter MA. 2000. Measles virus matrix protein specifies apical virus release and glycoprotein sorting in epithelial cells. EMBO J 19:3576–3585. https://doi.org/10.1093/emboj/19.14.3576.
53. Tahara M, Takeda M, Yanagi Y. 2007. Altered interaction of the matrix protein with the cytoplasmic tail of hemagglutinin modulates measles virus growth by affecting virus assembly and cell-cell fusion. J Virol 81:6827–6836. https://doi.org/10.1128/JVI.00248-07.

54. Liljeroos L, Huiskonen JT, Ora A, Susi P, Butcher SJ. 2011. Electron cryotomography of measles virus reveals how matrix protein coats the ribonucleocapsid within intact virions. Proc Natl Acad Sci U S A 108:18085–18090. https://doi.org/10.1073/pnas.1105770108.
55. Money VA, McPhee HK, Mosely JA, Sanderson JM, Yeo RP. 2009. Surface features of a Mononegavirales matrix protein indicate sites of membrane interaction. Proc Natl Acad Sci U S A 106:4441–4446. https://doi.org/10.1073/pnas.0805740106.
56. Leyrat C, Renner M, Harlos K, Huiskonen JT, Grimes JM. 2014. Structure and self-assembly of the calcium binding matrix protein of human metapneumovirus. Structure 22:136–148. https://doi.org/10.1016/j.str.2013.10.013.
57. Liu YC, Grusovin J, Adams TE. 2018. Electrostatic interactions between Hendra virus matrix proteins are required for efficient virus-like-particle assembly. J Virol 92:e00143-18. https://doi.org/10.1128/JVI.00143-18.
58. Forster A, Maertens GN, Farrell PJ, Bajorek M. 2015. Dimerization of matrix protein is required for budding of respiratory syncytial virus. J Virol 89:4624–4635. https://doi.org/10.1128/JVI.03500-14.
59. Bringolf F, Herren M, Wyss M, Vidondo B, Langedijk JP, Zurbriggen A, Plattet P. 2017. Dimerization efficiency of canine distemper virus matrix protein regulates membrane-budding activity. J Virol 91:e00521-17. https://doi.org/10.1128/JVI.00521-17.
60. McPhee HK, Carlisle JL, Beeby A, Money VA, Watson SM, Yeo RP, Sanderson JM. 2011. Influence of lipids on the interfacial disposition of respiratory syncytical virus matrix protein. Langmuir 27:304–311. https://doi.org/10.1021/la104041n.
61. Ke Z, Strauss JD, Hampton CM, Brindley MA, Dillard RS, Leon F, Lamb KM, Plemper RK, Wright ER. 2018. Promotion of virus assembly and organization by the measles virus matrix protein. Nat Commun 9:1736. https://doi.org/10.1038/s41467-018-04058-2.
62. Watkinson RE, Lee B. 2016. Nipah virus matrix protein: expert hacker of cellular machines. FEBS Lett 590:2494–2511. https://doi.org/10.1002/1873-3468.12272.
63. Subhashri R, Shaila MS. 2007. Characterization of membrane association of rinderpest virus matrix protein. Biochem Biophys Res Commun 355:1096–1101. https://doi.org/10.1016/j.bbrc.2007.02.088.
64. Caldwell SE, Lyles DS. 1986. Dissociation of newly synthesized Sendai viral proteins from the cytoplasmic surface of isolated plasma membranes of infected cells. J Virol 57:678–683. https://doi.org/10.1128/JVI.57.2.678-683.1986.
65. Gc JB, Gerstman BS, Chapagain PP. 2017. Membrane association and localization dynamics of the Ebola virus matrix protein VP40. Biochim Biophys Acta Biomembr 1859:2012–2020. https://doi.org/10.1016/j.bbamem.2017.07.007.
66. Del Vecchio K, Frick CT, Gc JB, Oda SI, Gerstman BS, Saphire EO, Chapagain PP, Stahelin RV. 2018. A cationic, C-terminal patch and structural rearrangements in Ebola virus matrix VP40 protein control its interactions with phosphatidylserine. J Biol Chem 293:3335–3349. https://doi.org/10.1074/jbc.M117.816280.
67. Johnson KA, Taghon GJ, Scott JL, Stahelin RV. 2016. The Ebola virus matrix protein, VP40, requires phosphatidylinositol 4,5-bisphosphate (PI(4,5)P2) for extensive oligomerization at the plasma membrane and viral egress. Sci Rep 6:19125. https://doi.org/10.1038/srep19125.
68. Wijesinghe KJ, Stahelin RV. 2016. Investigation of the lipid binding properties of the Marburg virus matrix protein VP40. J Virol 90:3074–3085. https://doi.org/10.1128/JVI.02607-15.
69. Koehler A, Pfeiffer S, Kolesnikova L, Becker S. 2018. Analysis of the multifunctionality of Marburg virus VP40. J Gen Virol 99:1614–1620. https://doi.org/10.1099/jgv.0.001169.
70. Jasenosky LD, Neumann G, Lukashevich I, Kawaoka Y. 2001. Ebola virus VP40-induced particle formation and association with the lipid bilayer. J Virol 75:5205–5214. https://doi.org/10.1128/JVI.75.11.5205-5214.2001.
71. Ruigrok RW, Schoehn G, Dessen A, Forest E, Volchkov V, Dolnik O, Klenk HD, Weissenhorn W. 2000. Structural characterization and membrane binding properties of the matrix protein VP40 of Ebola virus. J Mol Biol 300:103–112. https://doi.org/10.1006/jmbi.2000.3822.
72. Mohamad Yusoff MA, Abdul Hamid AA, Mohammad Bunori N, Abd Halim KB. 2018. Interaction of monomeric Ebola VP40 protein with a plasma membrane: a coarse-grained molecular dynamics (CGMD) simulation study. J Mol Graph Model 82:137–144. https://doi.org/10.1016/j.jmgm.2018.04.010.
73. Sanchez-Serrano I. 2006. Success in translational research: lessons from the development of bortezomib. Nat Rev Drug Discov 5:107–114. https://doi.org/10.1038/nrd1959.
74. Lim KL, Chew KC, Tan JM, Wang C, Chung KK, Zhang Y, Tanaka Y, Smith W, Engelender S, Ross CA, Dawson VL, Dawson TM. 2005. Parkin mediates nonclassical, proteasomal-independent ubiquitination of synphilin-1: implications for Lewy body formation. J Neurosci 25:2002–2009. https://doi.org/10.1523/JNEUROSCI.4474-04.2005.
75. Buchholz UJ, Finke S, Conzelmann KK. 1999. Generation of bovine respiratory syncytial virus (BRSV) from cDNA: BRSV NS2 is not essential for virus replication in tissue culture, and the human RSV leader region acts as a functional BRSV genome promoter. J Virol 73:251–259. https://doi.org/10.1128/JVI.73.1.251-259.1999.